JOURNAL OF PETROLOGY | VOLUME 48 | NUMBER 4 | PAGES 711–728 | 2007 | doi:10.1093/petrology/egl079

Using LA-ICPMS Mapping and Sector Zonation to Understand Growth and Trace-Element Partitioning in Sector-Zoned Clinopyroxene Oikocrysts from the Norra Ulvö Gabbro, Sweden

D. T. CLAESON[1]*, W. P. MEURER[2], K. J. HOGMALM[3] AND S.-Å. LARSON[3]

[1]GEOLOGICAL SURVEY OF SWEDEN, KILIANSGATAN 10, SE-223 50 LUND, SWEDEN

[2]EXXONMOBIL UPSTREAM RESEARCH COMPANY, P.O. BOX 2189, HOUSTON, TX 77252-2189, USA

[3]EARTH SCIENCES CENTRE, GÖTEBORG UNIVERSITY, BOX 460, SE-405 30 GÖTEBORG, SWEDEN

RECEIVED MAY 24, 2006; ACCEPTED DECEMBER 19, 2006; ADVANCE ACCESS PUBLICATION FEBRUARY 9, 2007

Petrographic analysis and geochemical mapping are used to characterize sector-zoned clinopyroxene oikocrysts from the Norra Ulvö Gabbro, Sweden. The sector zones are distinguished optically and by differences in TiO_2, Al_2O_3, and incompatible trace elements. The oikocrysts grew with a branching morphology as evidenced by numerous triple points in a single oikocryst. Oikocrysts grew from the center of domains outward and the growth within individual domains did not completely fill the space until the oikocryst had reached its full size. In some domains sector zones are overgrown by growth zones that lack sectors. The last crystallization infilled channels that allowed late-stage liquids to move through the oikocryst at the contacts with chadacrysts. Calculation of partitioning behavior of trace elements between adjacent sectors shows it to be regular and consistent with experimental results. The data show that the $CaTiAl_2O_6$ component greatly enhances the solubility of most incompatible elements in clinopyroxene.

KEY WORDS: *cumulate; layered intrusion; oikocryst; sector-zoned; trace elements*

INTRODUCTION

Clinopyroxene is a common mineral in both terrestrial and lunar basaltic rocks. It has relatively high concentrations of most trace elements and is therefore useful in studies of diverse processes including cooling rates, mantle melting, fractional crystallization, and time scales of crystal residence in magma chambers (e.g. Kushiro, 1973; Dowty *et al.*, 1974; Skulski *et al.*, 1994; Van Orman *et al.*, 1998; Dobosi & Jenner, 1999; Hawkesworth *et al.*, 2004; Morgan *et al.*, 2004). The ability of clinopyroxene to grow as sector-zoned crystals has attracted attention, partly because partitioning of elements and kinetics related to crystal growth can be studied and partly because of its impact on petrogenetic models (e.g. Hollister & Gancarz, 1971; Nakamura, 1973; Bergantz, 1995). Sector-zoned clinopyroxene crystals are found in alkaline lavas and shallow intrusions (e.g. Leung, 1974) but rarely crystallize from calc-alkaline (Brophy *et al.*, 1999) or peralkaline magmas (Larsen, 1981). Published studies of sector-zoned clinopyroxene have focused on more or less euhedral grains occurring as phenocrysts in lavas or experimentally grown crystals. Here we provide the first detailed description of sector-zoned oikocrysts of clinopyroxene. These crystals are found throughout the layered stratigraphy of the Norra Ulvö Gabbro, Sweden.

How oikocrysts grow is an outstanding question in petrology (e.g. Mathison, 1987; Tegner & Wilson, 1995; Meurer & Claeson, 2002) and knowledge of their growth mechanism(s) provides a window into the postcumulus evolution of basaltic liquids (e.g. Claeson & Meurer, 2004). The presence of sector zonation in clinopyroxene

*Corresponding author. E-mail: dick.claeson@sgu.se

oikocrysts provides insights into how the crystals grew. Chemical mapping of the trace-element variation of sector-zoned oikocrysts sheds additional light on their style of growth. Here we use petrographic characterization and detailed chemical mapping of oikocrysts from four samples from the Norra Ulvö Gabbro to develop a conceptual model for their growth. We also use the chemical data to examine how variations in minor components (Al, Ti, Na) in the clinopyroxene influence trace-element partitioning in clinopyroxene.

PETROGRAPHIC AND BSE CHARACTERIZATION

The Norra Ulvö Gabbro is an alkali olivine basaltic sill that intruded continental crust at ~1·25 Ga (Welin & Lundqvist, 1975; Gorbatschev *et al.*, 1979; Lundqvist, 1990; Elming & Mattsson, 2001; Hogmalm *et al.*, 2006). It is part of the Ulvö Gabbro Complex, which is composed of a series of saucer-shaped intrusions with a diameter of ~30–80 km (Fig. 1). Ulvö is also known for being the type locality for ulvöspinel (Mogensen, 1946). Our samples were collected from a nearly complete section at Norra Ulvön, representing an estimated maximum thickness of 300 m with an emplacement depth of 2·5–3 km (Larson & Magnusson, 1976, 1979; Larson, 1980). The Norra Ulvö Gabbro consists of three zones: a lower zone (LZ), a rhythmically layered zone (RZ), and an upper zone (UZ; Fig. 1). The RZ is subdivided into RZa, which contains sector-zoned clinopyroxene oikocrysts, and RZb, which contains granular clinopyroxene. No clinopyroxene oikocrysts were formed after clinopyroxene appears as a granular mineral in the intrusion (RZb). The granular clinopyroxene is also sector zoned, but locally is recrystallized under magmatic conditions producing patchy chemical zonation.

The crystallization sequence of cumulus minerals in the Norra Ulvö Gabbro is olivine and plagioclase followed by ulvöspinel and then clinopyroxene (cumulus clinopyroxene is found only in RZb). These minerals are found in all cumulates. Accessory minerals found in most samples include apatite and biotite, which crystallize relatively early, and minor amounts of K-feldspar, albite, allanite, and

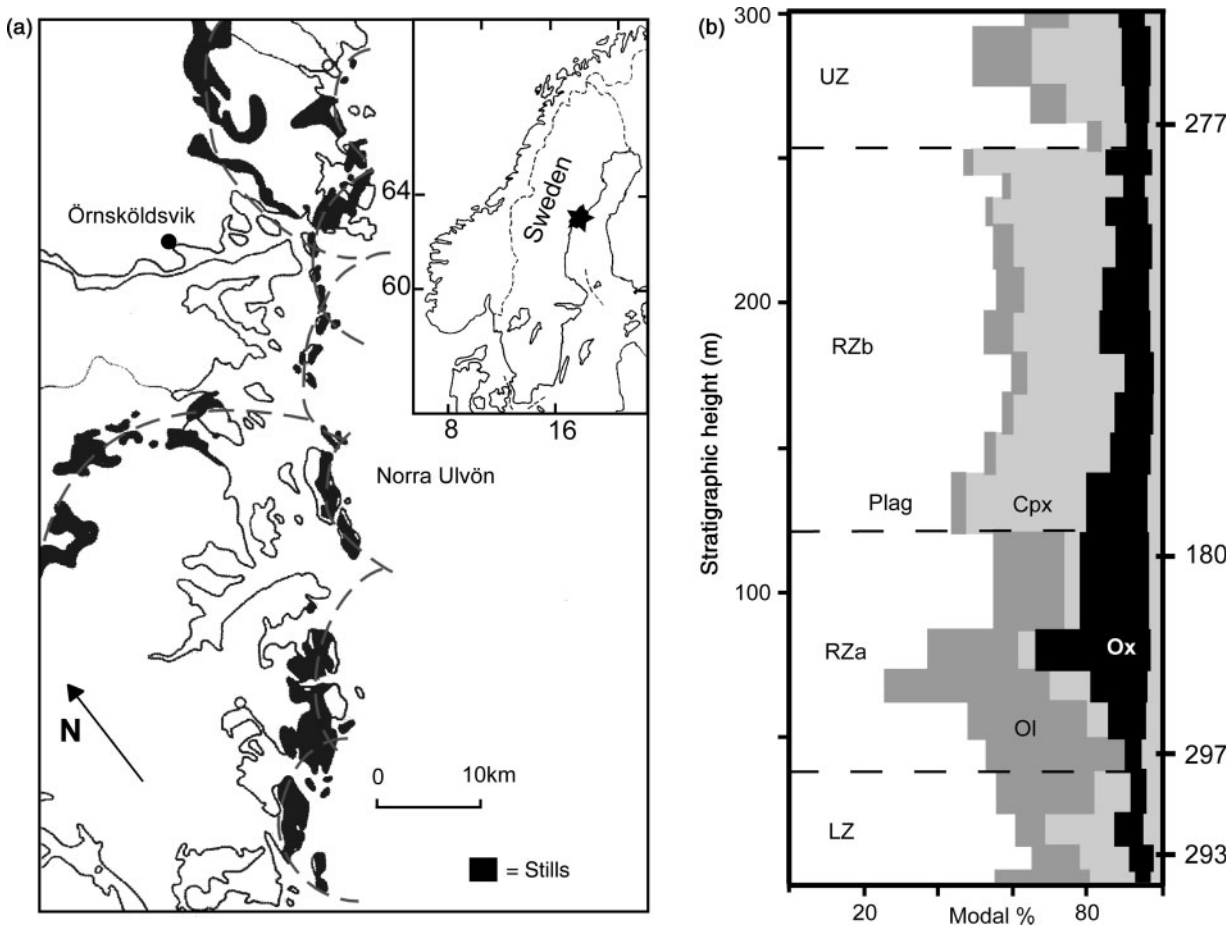

Fig. 1. (a) Location map of the Norra Ulvö Gabbro. (b) Stratigraphy of the Norra Ulvö Gabbro showing the locations of the studied samples. Numbers to the right in (b) are sample numbers.

baddeleyite, which are found in discrete interstitial spaces. Single clinopyroxene oikocrysts have a maximum size of ~50 mm and the maximum size of their domains is ~5 mm across. In this paper we use the term 'oikocryst' in the standard way to refer to relatively large crystals that poikilitically enclose numerous smaller crystals of other minerals (chadacrysts). Oikocrysts are recognized in hand sample by their uniform cleavage surfaces. In thin-section they are recognized as single grains by their optical continuity despite the fact that they are not contiguous in the section plane. Oikocrysts are composed of discrete domains that are isolated from each other by other minerals in the section plane. Domains are divided into one or more zones that are the distinct growth sector zones. The zones are distinct both optically and in back-scattered electron (BSE) images (Figs 2–4). The color in plane-polarized light varies from pink–light brown to dark brown, and to olive. The sharp internal boundaries in domains, defined by color variation, correspond to jumps in composition (mainly in Ti, Al, and some trace elements—see below). Triple and quadruple junctions between three and four zones (Fig. 4b) with different chemical compositions, in a single domain, show the level of chemical complexity present.

In some domains the sector zones are overgrown by non-sector-zoned clinopyroxene (Fig. 4). We refer to this overgrowth process as growth zonation and to its product as growth zones. The growth zones are optically distinct and well defined in BSE images. They have less TiO_2 and more FeO than the sector-zoned parts of the same domain (see below). The final crystallization of the oikocrysts is restricted to small discrete blebs located adjacent to chadacrysts that are distinct in BSE images but can be either brighter (higher mean atomic number) or darker (lower mean atomic number) than the rest of the oikocryst. As described below, these blebs have the highest concentrations of incompatible trace elements in any part of a given oikocryst.

We found no textural evidence (or chemical evidence as described below) that the chadacrysts reacted with the liquid during growth of clinopyroxene oikocrysts (Fig. 3c; see Meurer & Claeson, 2002). However, Larson (1980) noted the presence of rounded olivine in some clinopyroxene oikocrysts and suggested that these were partially resorbed. Boundaries between oikocrysts and other interstitial minerals (apatite and biotite) are smooth and most are straight. Apatite crystals included in the oikocrysts are euhedral to subhedral and found in domains near the oikocryst margins (Figs 3 and 4).

ANALYTICAL METHODS AND RESULTS

The clinopyroxene in four samples (277, 180, 297, 293) were studied using laser-ablation inductively coupled plasma mass spectrometry (LA-ICPMS) analysis and electron microscopy. These samples span the stratigraphy of the intrusion (Fig. 1). All analyses were conducted at the Earth Sciences Centre, Göteborg University. Major elements were determined using a Zeiss® DSM 940 scanning electron microscope with a Link® energy-dispersive spectrometry (EDS) system. We used an accelerating voltage of 25 kV, a sample current of ~1 nA, a counting livetime of 100 s, and calibrated with natural minerals and simple oxide standards. Cobalt was used as a reference standard and to minimize drift. Raw counts were reduced using a ZAF correction. Based on comparisons with wavelength-dispersive spectrometry analyses using microprobes at Duke University and the University of Houston, estimated uncertainties in our EDS analyses are ~1% relative for most elements with detection limits ~0·1%. Trace-element concentrations were determined by LA-ICPMS using a Cetac ASX-200 Nd–YAG UV laser for sampling and a HP-4500 quadrupole ICP-MS system for analysis. Spots of 100 μm diameter were sampled using a laser repetition rate of 5 Hz and spots of 50 μm diameter were sampled at 10 Hz with a laser power of ~5 mJ in both cases. All sections analyzed were prepared at ~100 μm thickness. NIST 612 glass was used as a standard and the raw counts were reduced using procedures detailed by Meurer & Claeson (2002). Estimated precision is approximately dependent upon elemental concentrations as follows: ≥10 ppm (better than 5%), 0·25–10 ppm (≤10%), 0·05–0·25 ppm (≤20%) and <0·05 ppm (~20–50%).

Major-element composition of clinopyroxene oikocrysts

The clinopyroxene from the Ulvö gabbro is augite with wollastonite (40–45%), enstatite and ferrosilite components accounting for ~93% of the total (Table 1; see also Electronic Appendix 1, which is available for downloading from http://www.petrology.oxfordjournals.org). The remaining, non-quadrilateral components are predominantly TiO_2 and Al_2O_3 with subordinate Na_2O. The sector zonation observed optically corresponds most closely to variations in TiO_2 and Al_2O_3. The Mg-number varies systematically between sectors, but whereas TiO_2 and Al_2O_3 can vary by a factor of two or more between sectors, the Mg-number typically varies by only 5–10%. Zones that have high concentrations of TiO_2 and Al_2O_3 have lower relative Mg-number. Only minor variability is found in Na_2O, CaO, SiO_2, and MnO concentrations between sectors.

We summarize the compositional variation of the oikocrysts using bubble plots (Fig. 5). These plots depict the position of each analysis in a scaled map (the $x-y$ coordinates). The size of each bubble (data point) is scaled to the concentration it represents. Rather than plotting the raw concentration data, which would

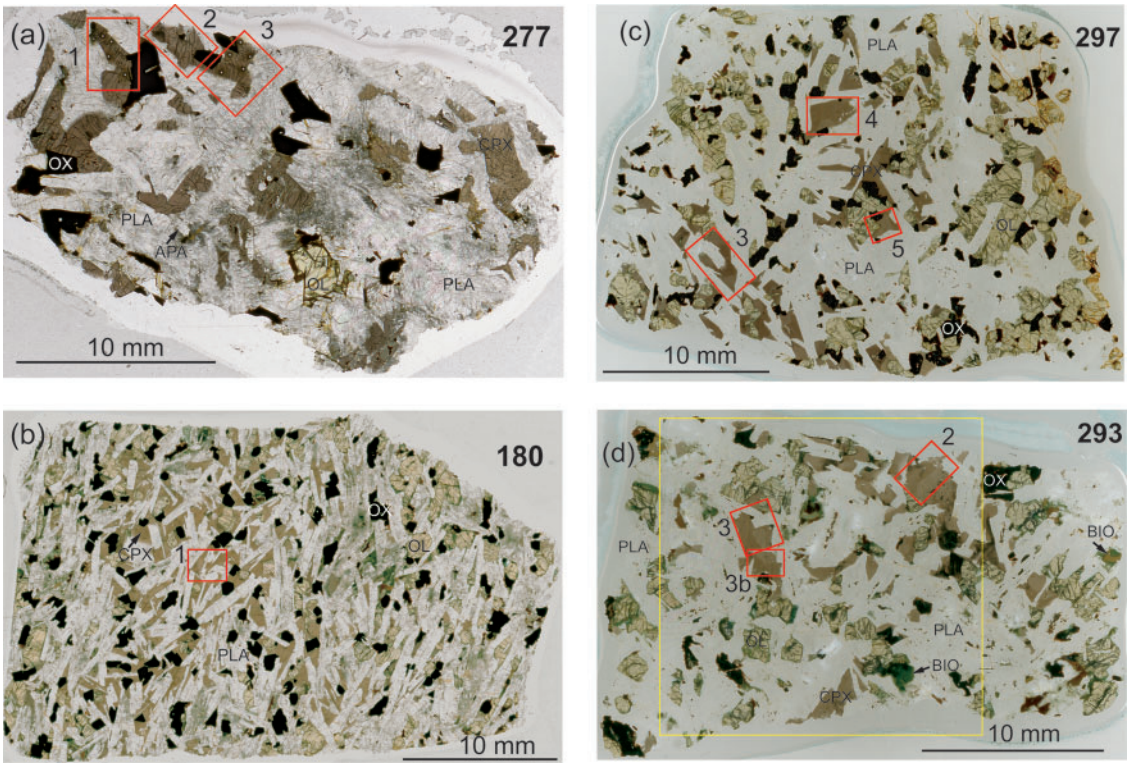

Fig. 2. Plane-polarized light photomicrographs of entire thin-sections (~100 μm thick). Red boxes denote locations of BSE images and areas used for LA-ICPMS sampling. The yellow box in (d) encloses the oikocryst used in Figs 6 and 10.

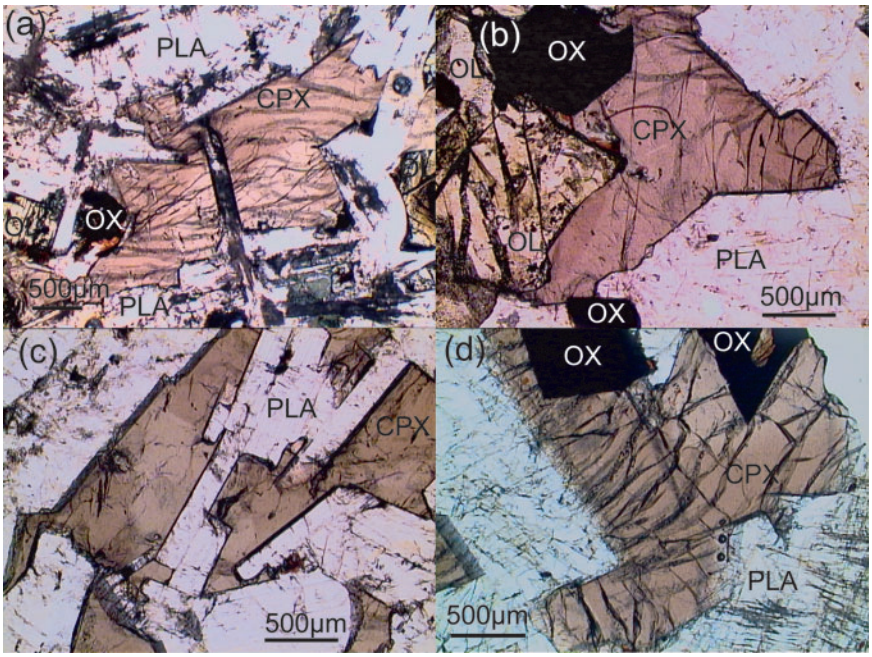

Fig. 3. Plane-polarized light photomicrographs of domains in clinopyroxene oikocrysts from ~100 μm thick sections: (a) 293cpx3 from the LZ; (b) 297cpx5 from the lower part of RZa; (c) 180cpx1 from the upper part of RZa; (d) 277cpx3 from the UZ.

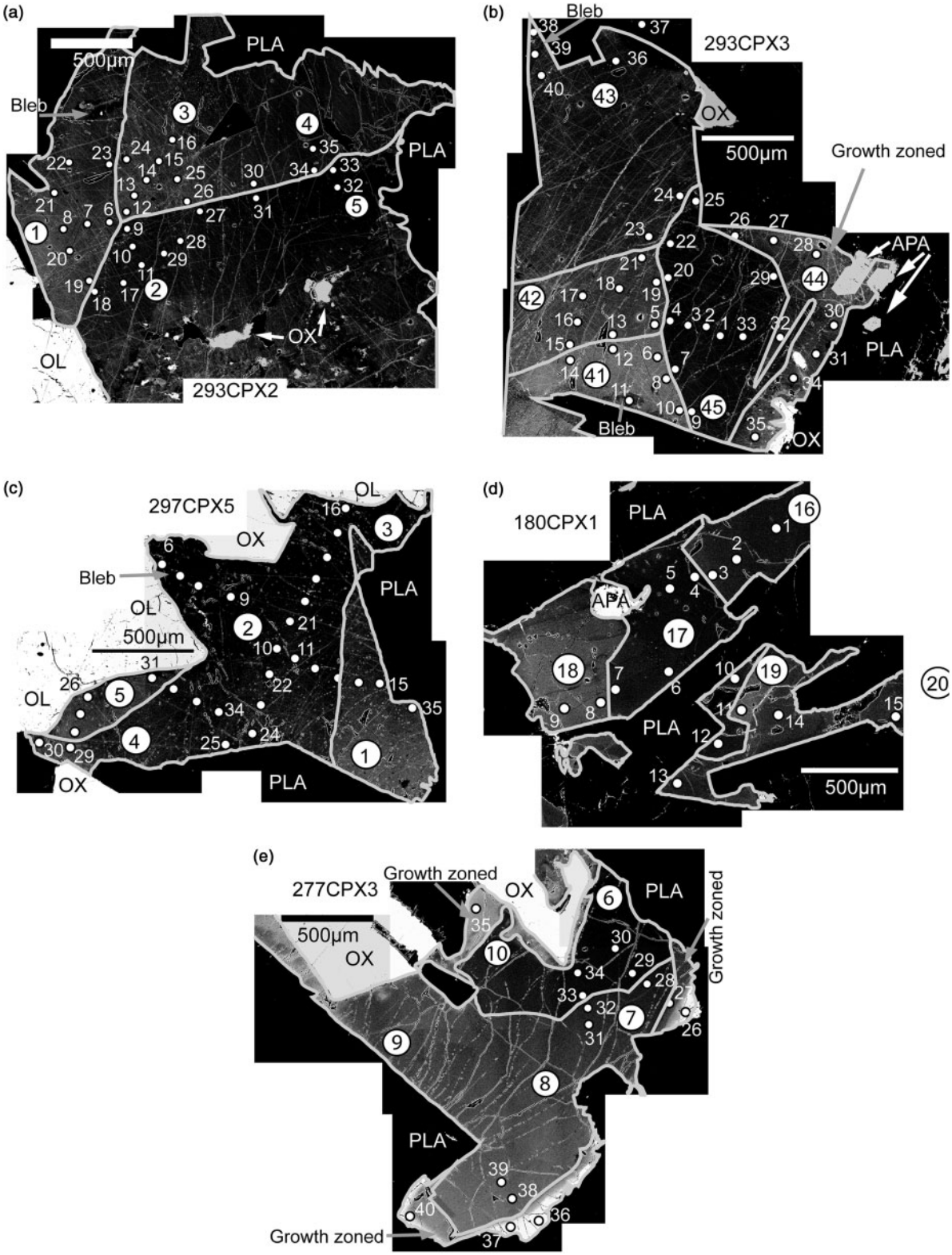

Fig. 4. Mosaics of back-scattered electron (BSE) images for selected domains in clinopyroxene oikocrysts. Minerals, internal sectors, growth zonation, and blebs are all labeled and locations indicated with arrows where appropriate. (a) 293cpx2 and (b) 293cpx3 from the LZ; (c) 297cpx5 from the lower part of RZa; (d) l80cpxl from the upper part of RZa; (e) 277cpx3 from the UZ. Numbers correspond to LA-ICPMS analyses and actual spot size (50 and l00 μm) is shown with white circles. These images were used to create outlines in Fig. 5.

Table 1: Representative SEM-EDS analyses of clinopyroxene

Sample no.	SiO_2	TiO_2	Al_2O_3	FeO	MnO	MgO	CaO	Na_2O	Sum	Mg-no.	100 μm spot*
180cpx1-34	49·55	1·76	3·47	10·79	0·18	12·78	20·27	0·51	99·31	67·85	180cpx1-16
180cpx1-35	49·94	1·81	3·61	10·96	0·26	12·88	20·59	0·44	100·49	67·68	180cpx1-16
180cpx1-17	51·73	1·20	2·42	10·63	0·21	13·78	20·37	0·43	100·76	69·79	180cpx1-17
180cpx1-30	51·22	1·23	2·19	10·36	0·24	13·66	20·42	0·52	99·83	70·16	180cpx1-17
180cpx1-12	49·86	1·93	3·67	10·95	0·21	12·96	20·71	0·38	100·68	67·83	180cpx1-18
180cpx1-27	49·89	1·77	3·75	10·81	0·23	13·00	20·25	0·45	100·16	68·19	180cpx1-18
277cpx1-27	50·75	1·16	2·03	13·28	0·29	11·18	20·34	0·37	99·39	60·01	277cpx1-3
277cpx1-28	51·29	0·63	1·43	15·00	0·46	10·86	19·82	0·40	99·89	56·34	277cpx1-3
277cpx3-10	51·78	1·08	1·74	12·28	0·33	12·60	20·44	0·48	100·73	64·65	277cpx3-6
277cpx3-21	50·78	1·40	2·43	12·50	0·34	12·32	20·32	0·49	100·57	63·73	277cpx3-7
277cpx3-23	50·39	1·47	2·64	12·33	0·28	12·40	20·21	0·51	100·23	64·18	277cpx3-8
277cpx3-27	50·69	1·49	2·53	12·40	0·38	12·43	20·16	0·54	100·61	64·12	277cpx3-8
277cpx3-33	51·49	1·17	1·79	12·04	0·32	12·81	20·10	0·49	100·21	65·48	277cpx3-10
277cpx3-36	51·50	1·07	1·73	12·16	0·28	12·73	19·93	0·57	99·98	65·11	277cpx3-10
293cpx2-19	49·92	1·68	2·92	10·51	0·22	13·27	20·45	0·55	99·52	69·23	293cpx2-1
293cpx2-80	50·43	1·69	3·03	10·73	0·20	13·10	20·68	0·55	100·41	68·52	293cpx2-1
293cpx2-16	51·51	1·31	2·18	10·58	0·30	13·80	20·36	0·52	100·55	69·94	293cpx2-2
293cpx2-17	51·61	1·37	2·27	10·57	0·25	13·63	20·25	0·47	100·41	69·69	293cpx2-2
293cpx2-50	50·22	1·81	3·12	10·83	0·24	13·11	20·44	0·43	100·20	68·33	293cpx2-3
293cpx2-52	49·73	1·80	3·32	10·86	0·25	12·92	20·45	0·42	99·76	67·96	293cpx2-3
293cpx2-54	49·53	1·96	3·43	10·91	0·28	12·79	20·18	0·47	99·55	67·63	293cpx2-4
293cpx2-59	51·48	1·38	2·31	10·44	0·26	13·48	20·58	0·48	100·43	69·70	293cpx2-5
293cpx3-21	49·78	1·95	2·87	11·53	0·25	12·65	20·04	0·60	99·68	66·16	293cpx3-41
293cpx3-4	51·23	1·24	1·76	11·02	0·32	13·44	20·25	0·57	99·83	68·48	293cpx3-45
297cpx5-4	50·35	1·77	2·92	10·38	0·22	13·42	20·31	0·57	99·95	69·73	297cpx5-1
297cpx5-18	50·62	1·76	2·97	10·27	0·24	13·33	20·54	0·53	100·26	69·82	297cpx5-1
297cpx5-33	51·37	1·30	2·01	10·03	0·29	14·06	20·20	0·51	99·77	71·42	297cpx5-2
297cpx5-36	51·62	1·30	2·04	10·26	0·25	14·01	19·92	0·55	99·95	70·89	297cpx5-2
297cpx5-40	51·50	1·25	2·12	10·23	0·24	13·90	20·36	0·55	100·16	70·77	297cpx5-4
297cpx5-25	50·88	1·65	2·73	10·09	0·24	13·64	20·41	0·59	100·24	70·68	297cpx5-5
297cpx5-26	51·46	1·39	2·22	10·23	0·21	13·96	20·32	0·52	100·31	70·87	297cpx5-5

Sample numbers: e.g. 293cpx2-1 is sample 293, domain 2, analysis 1.
*Corresponding sector of 100 μm spots from Table 2.

generate similar-sized bubbles in most instances, we subtract (or renormalize) the data either to the average concentration of the entire dataset for that sample or to some other significant concentration so that the bubble plots shows a range of concentrations relative to this value. Concentrations close to the selected value are depicted as small symbols and those that deviate more significantly are shown as increasingly larger bubbles. Values less than the normalizing value are plotted as open symbols and those greater than the normalizing value as filled symbols. In each bubble plot the normalizing value is given and the relative concentrations for selected bubbles of different sizes are provided next to the bubbles.

The major element composition of a clinopyroxene oikocryst in sample 293 was mapped in detail (277 analyses) to characterize its compositional variation (Fig. 6). The TiO_2 variation in the clinopyroxene provides a good measure of the progress of the crystallization of the interstitial liquid because it is depleted in the liquid by the co-crystallizing ulvöspinel. The Mg-number shows systematic variations with TiO_2 as defined by variations between sectors within a domain (Figs 6 and 7a). TiO_2 and Al_2O_3 are positively correlated at TiO_2 concentrations above ~1 wt % but below this concentration there is little or no decrease in the Al_2O_3 as TiO_2 decreases to near zero (Fig. 7b). TiO_2 and CaO show the opposite

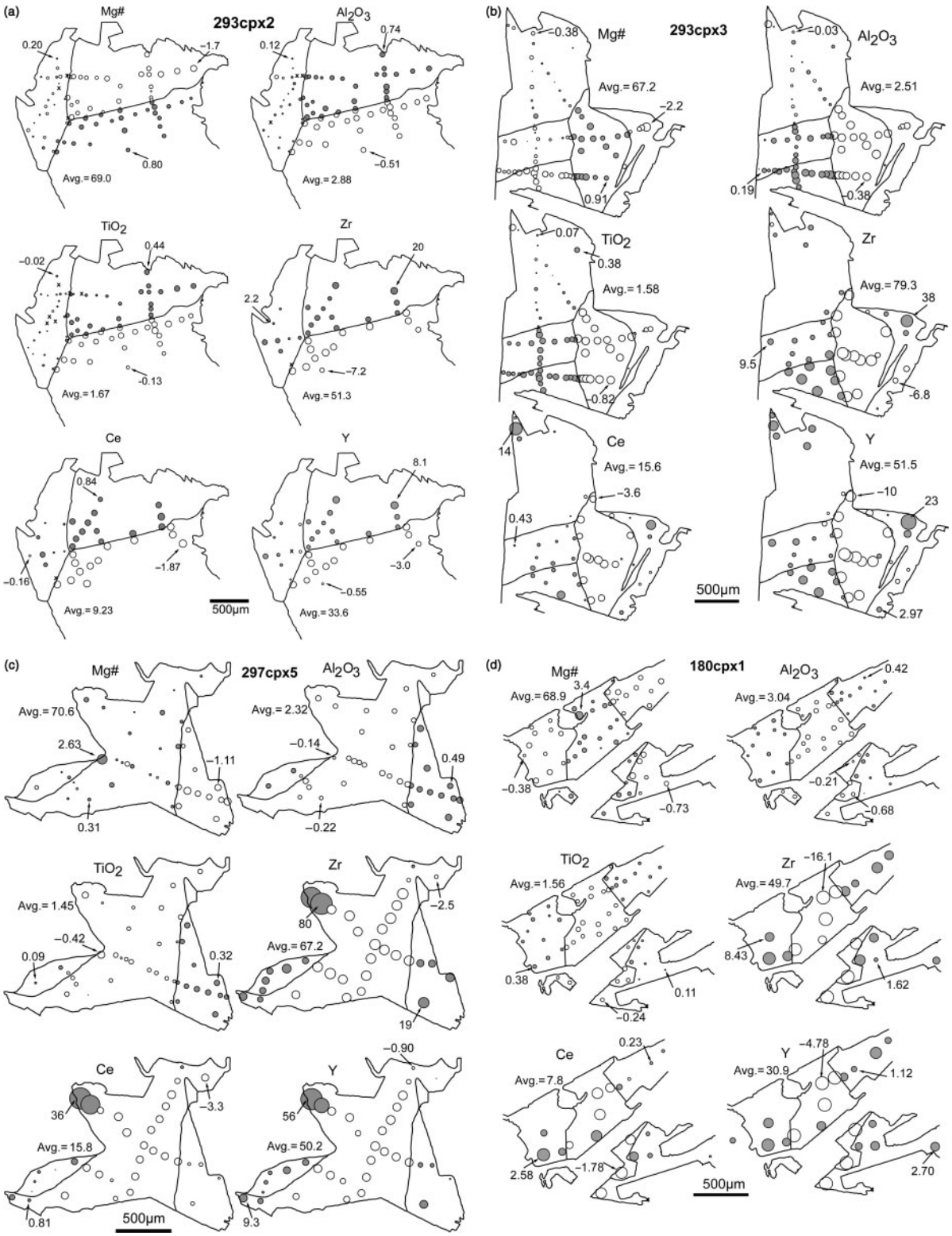

Fig. 5. Bubble plots of Mg-number, Al_2O_3, TiO_2, Zr, Ce, and Y on sketches of domain outlines in clinopyroxene oikocrysts. Sector boundaries within each domain are also shown (see Fig. 4). (a) 293cpx2; (b) 293cpx3; (c) 297cpx5; (d) 180cpx1; (e) 277cpx3. Extreme values of Zr, Y, and Ce found in 277cpx3 are plotted as squares without any size connotation (actual values are given in Electronic Appendix 3). Grey filled symbols have positive values and open symbols have negative values compared with calculated average (see text for explanation of how bubble plots are construed). × indicates a value so close to the average that its bubble size would not appear on the plot.

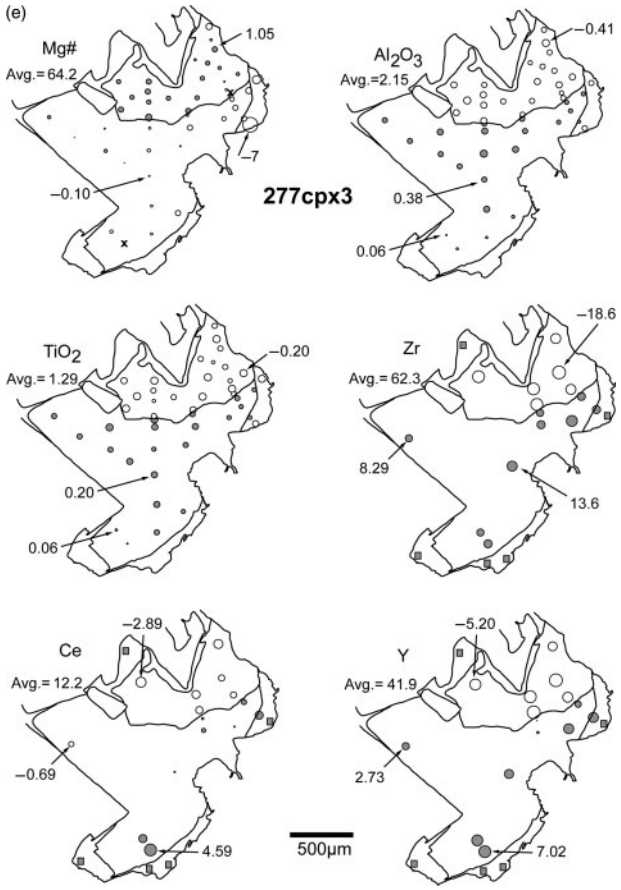

Fig. 5. Continued.

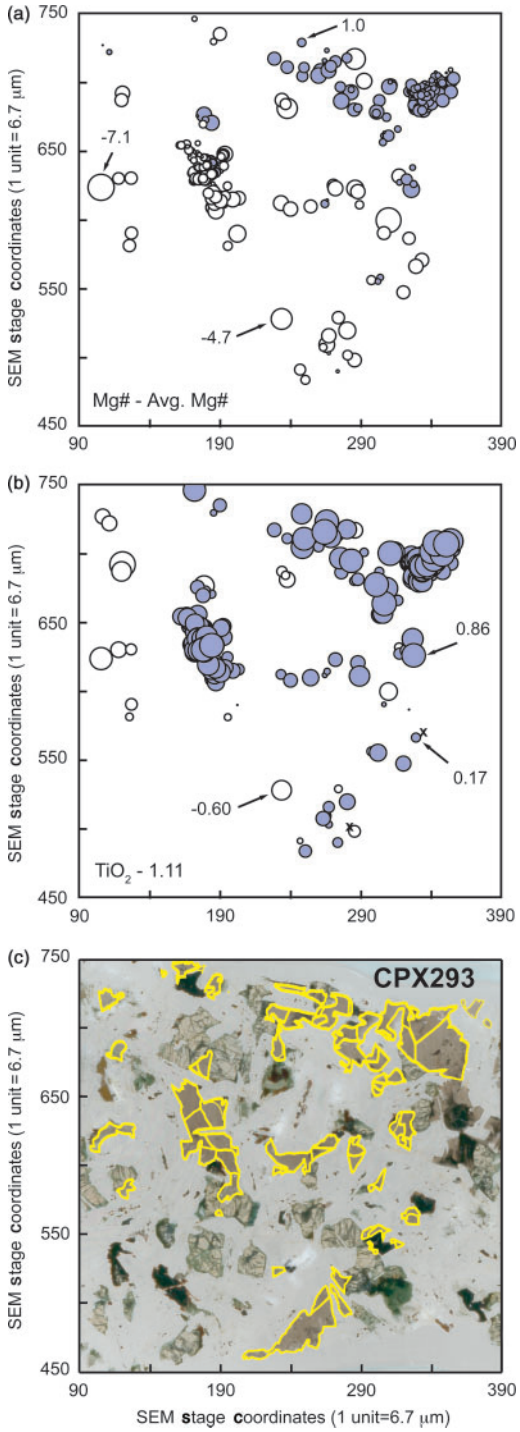

Fig. 6. Bubble plots of (a) the Mg-number and (b) the TiO_2 contents of an oikocryst from sample 293. In (b), –1·11 was chosen instead of average TiO_2 as no sector zonation is found in any domain that has maximum TiO_2 concentrations less than ~1·11 wt %. Filled symbols have positive values and open symbols have negative values (see text for explanation of how bubble plots are construed). × indicates a value so close to the normalizing that its bubble size would not appear on the plot. (c) The oikocryst shown in a plane-polarized light photomicrograph (see Fig. 2d) with outline in yellow showing the domain boundaries, internal sectors, and growth zones (Figs 4 and 5).

relation, with a well-defined negative correlation at low TiO_2 concentrations and essentially invariant CaO when TiO_2 is above ~1 wt % (Fig. 7c). Na_2O varies between ~0·4 and 0·6 wt % and is not correlated with TiO_2 (Fig. 7d).

The major-element variations that define the sector zonation (and the optical characteristics) are not present in the later crystallized parts of the oikocrysts. These parts include (in the order we interpret them to have formed): (1) overgrowths on sector-zoned portions of crystals; (2) domains that lack discrete sectors; (3) small regions at the margins of domains—the blebs described above. These three portions of the oikocrysts have relatively low TiO_2 and high CaO. The blebs are distinct in BSE images as areas that are distinctly light- or dark-colored relative to the adjacent area. They have the lowest concentrations of TiO_2 and Al_2O_3 compared with all zones in a domain or oikocryst. The Mg-number of the blebs may be higher or lower than, or equal to, that of the clinopyroxene that fills the bulk of their host domain (Fig. 5).

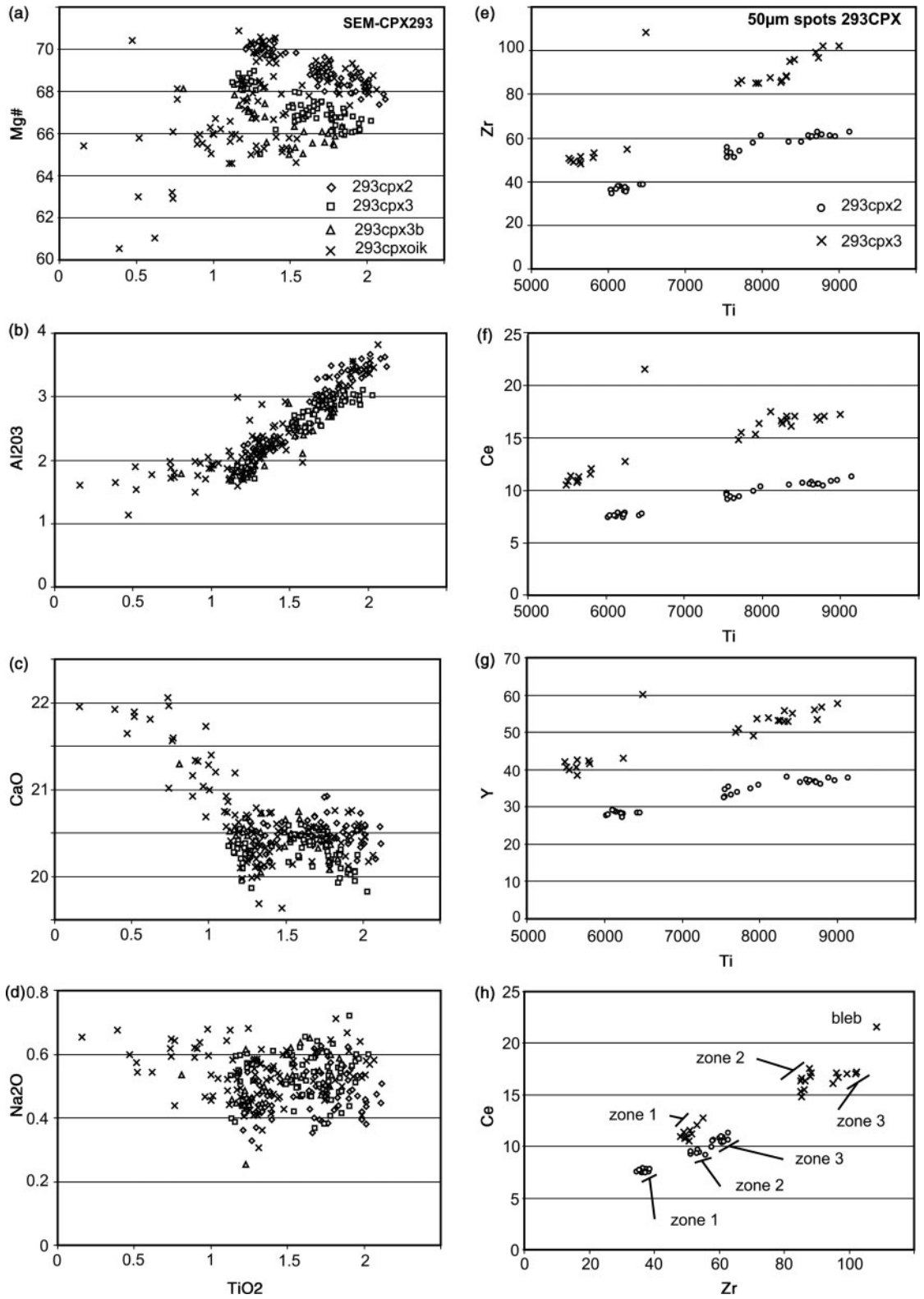

Fig. 7. Element–element plots for domains in a single oikocryst 293 from the LZ. (a–d) Major element variations are shown for multiple analyses from three domains and a scattered sampling of other domains from throughout the crystal. (e–h) Plots comparing trace-element variations between two domains. Analyses from individual sectors plots as discrete groups in Ce–Zr space and corresponding sectors between domains are labeled (Fig. 7h).

Trace-element compositions of clinopyroxene oikocrysts

Trace-element data were collected from 35 of the 100 μm spots and 172 of the 50 μm spots (Table 2; see also Electronic Appendices 2 and 3, available for downloading at http://www.petrology.oxfordjournals.org). Traverses of 50 μm spots were positioned to best examine: (1) sharp jumps in trace-element composition between zones; (2) the internal homogeneity of zones; (3) areas with extreme trace-element compositions. The 100 μm spots were used to characterize the oikocrysts for a larger set of elements than quantified with the 50 μm spots. The 100 μm spots were sampled after traverses of 50 μm spots and cleaning of surface debris.

Detailed mapping of domains with several sectors reveals correlations between minor and trace elements. The variations in Ce, Y, and Zr concentrations mimic those of TiO_2 and Al_2O_3 (Fig. 5). As with the major elements, the concentrations of the trace elements change abruptly across sector zones. For example, average Zr concentrations from each of three sectors at a triple point in sample 293cpx2 are 37, 52, and 61 ppm. Zr variations between zones in the other samples are similar (e.g. 47 and 71 ppm for sample 277cpx3; 35 and 60 ppm for sample 180cpx1; 52 and 77 ppm for sample 297cpx5). Most sectors are relatively homogeneous in both major- and trace-element contents except near their margins (Fig. 5).

We examined two domains of an oikocryst from sample 293 in detail to compare the trace-element variability between domains. Each domain has three sector zones (Figs 4 and 5). The 50 μm spots were used to map the variability in Zr, Ce, and Y, which are in turn used to describe how high field strength elements (HFSE), light rare earth elements (LREE), and heavy rare earth elements (HREE), respectively, are distributed in the domains. All three elements are positively correlated with Ti (Fig. 7). We use TiO_2 when referring to the major-element analyses (by SEM) and Ti when referring to the LA-ICPMS analyses. Although the concentrations are similar, they vary since the laser samples a larger volume. Each of the three sectors, in both domains, defines a separate group in Ti vs Zr, Ce, and Y space, where the higher Ti groups in 293cpx3 show some overlap with each other (Fig. 7). The three groups in each domain are well defined in Zr vs Ce space (Fig. 7h). Domain 293cpx2 has lower concentrations of Zr, Ce, and Y compared with 293cpx3, although both have similar Ti concentrations. Spot 293cpx3-11 is from an analysis of a bleb and falls off the trends defined by other analyses from this domain.

The trace-element concentrations can vary widely between the same sectors in different domains. Normalizing the trace-element concentrations to the Ti concentration makes it possible to correlate sectors between different domains. For example, in a Y/Ti vs Zr/Ti plot of two domains from sample 293, the individual domains define groups with a weak negative correlation whereas the sectors that correspond between the domains show parallel linear trends with positive slopes (Fig. 8d). It should be noted that although the analyses from two of the sectors show substantial overlap in this plot, it is still possible to correlate the sectors, as the data are grouped based on their locations as well. Similar relations are seen between sectors and domains for the other three samples (Fig. 8).

The 100 μm spots provide a more complete characterization of the trace-element variability within and between the clinopyroxene oikocrysts. For comparison we have normalized the analyses from each sample to an average clinopyroxene composition from the chilled margin of the sill. The resulting normalized variation diagrams show tight clustering for the transition metals (Sc, Ti, V, Mn, Co, Ni) and values near one except for Ni, which is depleted in all samples except 293 (Fig. 9). Sr values are also near one, with limited variation. All other elements show much more variability, but despite these variations, the patterns are sub-parallel. Zones that are easily distinguished optically and in BSE images are tightly grouped for most elements. Elements close to the detection limit (e.g. Th, U) show large within-sample variability.

The portions of the oikocrysts that are either sector zoned or growth zoned and richest in incompatible elements are invariably located at the margins of the domains. However, blebs always have the highest concentrations of incompatible elements for the domain in which they occur (e.g. 297cpx3-14 to cpx3-19, and cpx3-22 and -23). They also have higher concentrations than any other 'non-bleb' part of an oikocryst. For example, spot 277cpx1-3 has much higher concentrations of most incompatible elements and distinctly low concentrations of Sc, Ti, and V (Fig. 9). Similar compositional characteristics are found in other blebs (277cpx3-26, -35, -36, -37) in the same sample (Electronic Appendix 3). It should be noted that the Sr and Eu concentrations in these blebs are either depleted (Sr) or not notably enriched (Eu) compared with other analyses from this sample.

DISCUSSION

Characteristics of sector zonation

The cause of sector zoning in clinopyroxene may be related to differences in atomic structure and/or growth mechanisms for the different faces of the crystal. Adsorption of incompatible elements is preferentially concentrated in certain growth directions (e.g. Skulski *et al.*, 1994; Jensen, 2000). Most models for sector zoning in clinopyroxene have invoked high crystal growth rates as the fundamental cause. An examination of crystals that exhibit selective growth surfaces (e.g. titanite) reveals that even slowly grown crystals will display sector zonation when the

Table 2: Representative analyses of clinopyroxene: 100 μm spots (ppm)

Sample no.	Sc	Ti	V	Mn	Co	Ni	Rb	Sr	Y	Zr	Nb	Ba
180cpx1-16	229	8415	476	1594	39·3	30·2	0·04	29·7	32·4	57·9	0·06	0·30
180cpx1-17	198	6079	398	1678	41·8	33·7	0·07	26·5	26·2	34·8	0·02	0·10
180cpx1-18	229	8420	488	1613	40·9	32·7	0·02	29·9	33·7	58·2	0·07	0·46
277cpx1-3	128	3174	69	2892	37·5	13·1	0·23	21·4	188	294	0·22	3·03
277cpx3-6	163	5462	226	2043	39·1	15·6	0·04	29·6	38·3	50·5	0·05	0·15
277cpx3-7	182	7047	253	2012	37·8	13·9	0·02	33·4	47·2	77·6	0·10	0·18
277cpx3-8	185	7458	274	2039	38·7	16·0	0·02	34·4	46·3	75·9	0·10	0·35
277cpx3-10	169	5497	227	2047	39·7	18·4	0·02	29·1	36·7	47·0	0·05	0·14
293cpx2-1	186	8227	329	1536	34·8	48·9	0·04	43·4	38·3	61·0	0·07	0·32
293cpx2-2	184	6645	306	1666	38·5	52·9	0·01	27·6	33·1	44·0	0·02	0·08
293cpx2-3	210	8924	381	1564	36·6	52·6	0·00	33·6	41·3	66·0	0·06	0·30
293cpx2-4	220	9653	410	1591	38·2	53·3	b.d.l.	32·4	41·7	71·3	0·08	0·12
293cpx2-5	185	6781	315	1624	37·6	54·5	0·04	28·8	30·6	42·0	0·04	0·10
293cpx3-41	188	9454	324	1944	39·4	44·3	0·02	34·2	58·9	106	0·12	0·38
293cpx3-45	152	6043	243	1884	39·9	45·2	0·01	30·8	42·6	53·1	0·05	0·16
297cpx5-1	185	8395	344	1533	35·5	37·6	b.d.l.	34·2	58·4	86·6	0·09	0·19
297cpx5-2	162	6387	288	1689	38·0	39·7	b.d.l.	28·9	46·5	54·4	0·08	0·13
297cpx5-4	156	6263	276	1553	36·0	36·8	0·03	31·2	46·3	58·2	0·07	0·23
297cpx5-5	168	7736	327	1583	38·0	39·6	0·01	35·0	56·6	81·8	0·09	0·21

Sample no.	La	Ce	Nd	Sm	Eu	Gd	Dy	Er	Yb	Lu	Pb	Th	U
180cpx1-16	2·27	8·0	12·3	4·47	1·40	5·90	6·03	3·27	2·76	0·43	0·04	0·034	0·005
180cpx1-17	1·73	6·2	9·8	3·56	1·09	4·73	4·76	2·55	2·08	0·35	0·03	0·009	0·002
180cpx1-18	2·43	8·6	13·4	4·84	1·47	5·98	6·33	3·27	2·79	0·47	0·04	0·019	0·005
277cpx1-3	19·5	65·6	79·8	24·5	2·14	28·5	34·0	20·1	20·2	3·41	0·17	0·107	0·022
277cpx3-6	2·8	10·1	15·4	5·41	1·51	6·80	7·08	3·83	3·26	0·55	0·03	0·011	b.d.l.
277cpx3-7	3·3	12·4	19·0	6·53	1·81	8·40	8·58	4·67	4·06	0·66	0·03	0·013	b.d.l.
277cpx3-8	3·58	12·4	18·6	6·30	1·81	8·25	8·53	4·31	3·84	0·61	0·03	0·029	0·004
277cpx3-10	2·53	9·4	14·9	5·16	1·48	6·71	6·79	3·58	3·10	0·51	0·03	0·009	0·002
293cpx2-1	2·55	9·1	14·7	5·09	1·53	6·79	6·93	3·58	3·05	0·48	0·03	0·012	0·003
293cpx2-2	1·99	7·5	11·8	4·05	1·27	5·35	5·45	3·04	2·57	0·45	0·04	0·030	0·008
293cpx2-3	2·88	10·1	15·8	5·60	1·70	7·18	7·36	3·91	3·21	0·55	0·03	0·015	0·003
293cpx2-4	2·99	10·6	16·2	5·80	1·79	7·24	7·71	3·94	3·32	0·52	0·03	0·017	0·002
293cpx2-5	2·03	7·4	12·1	3·87	1·30	5·45	5·49	2·93	2·41	0·41	0·03	0·015	0·004
293cpx3-41	4·49	16·8	25·0	8·77	2·35	11·0	11·1	5·80	5·01	0·75	0·08	0·025	0·007
293cpx3-45	3·12	12·1	18·5	6·43	1·77	8·18	7·91	4·19	3·53	0·58	0·03	0·012	0·003
297cpx5-1	4·07	14·7	23·1	8·22	2·26	10·3	10·8	5·52	4·61	0·69	0·03	0·008	0·004
297cpx5-2	2·94	10·9	17·6	6·46	1·77	8·20	8·52	4·43	3·90	0·60	0·03	0·012	0·002
297cpx5-4	3·29	12·3	19·2	6·62	1·83	8·96	8·75	4·52	3·87	0·63	0·03	0·024	0·009
297cpx5-5	4·26	15·8	24·5	8·53	2·36	10·7	11·0	5·66	4·84	0·73	0·03	0·017	0·010

Sample numbers: e.g. 293cpx2-1 is sample 293, domain 2, analysis 1. b.d.l., below detection limit.

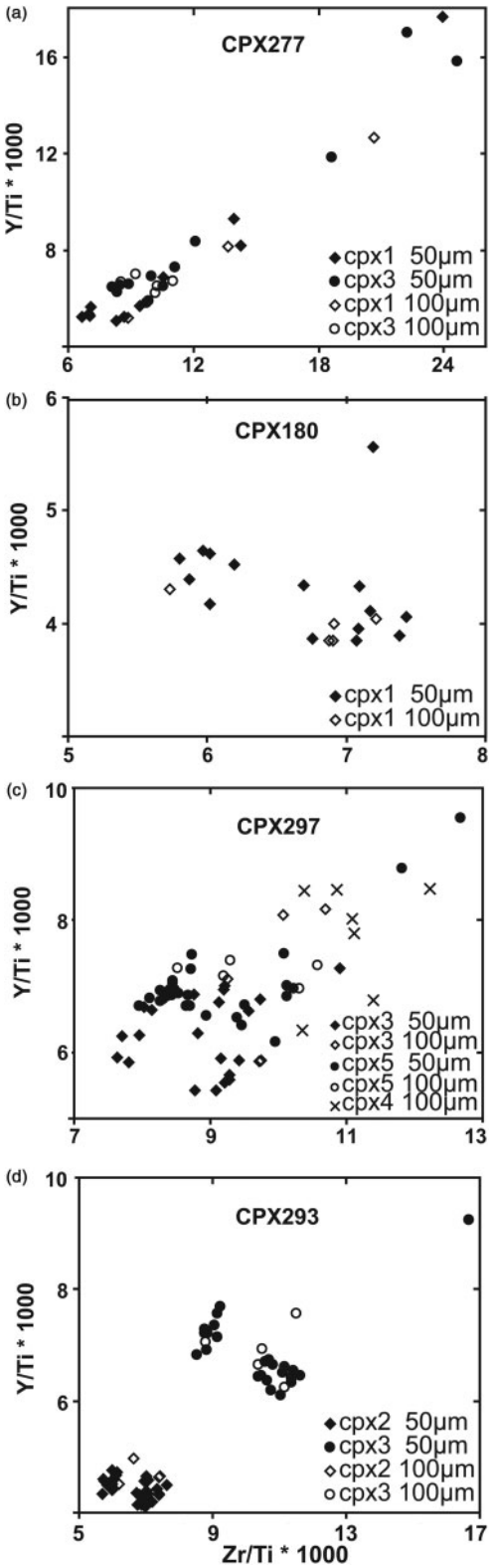

Fig. 8. Ratio plots of Zr/Ti vs Y/Ti in sector zones coded for each domain and for the size of the laser spot. For samples where multiple domains have been analyzed, corresponding sectors between domains plot as discrete groups and allow us to correlate them.

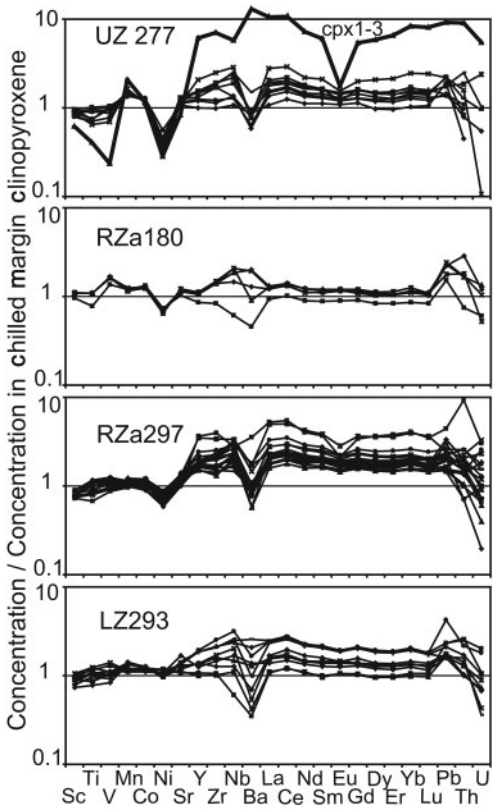

Fig. 9. Trace-element concentrations determined by 100 µm spots normalized to the average clinopyroxene composition from chilled margin samples. Spot 277cpx1-3 (labeled, and with bold line) is from a bleb.

growth rate exceeds the lattice diffusion rate within a near-surface layer (Watson & Liang, 1995).

Our detailed mapping provides some constraints on the conditions that prevailed during the growth of the sector-zoned clinopyroxene oikocrysts. Most domains are made up of sectors that are homogeneous (ignoring blebs) with regard to both major and trace elements (Fig. 5). This requires that the growth of the oikocryst did not exceed the diffusion rates of either major or trace elements through the liquid to the growing crystal faces. Early growth took place forming sector zones and was followed by normal growth zonation without sector zonation (e.g. Fig. 5b). Domains near the margins of oikocrysts show only normal growth zonation with distinct growth zones in BSE. The change from sector-zoned crystals to growth zonation suggests a change in the growth rate and/or some intensive parameter(s). Sector zonation may have been restricted to a period of relative undercooling during the early growth history of the clinopyroxene, followed by normal growth zonation. Alternatively, a relatively high liquid concentration of TiO_2 may be required to form sector zones and as its concentration falls below some threshold value, growth zonation takes

over. In sample 293 no sector zonation is found in any domain that has maximum TiO_2 concentrations less than ~1·11 wt %.

No diffusional homogenization of the oikocrysts is seen across the sharp internal boundaries that define the sector zones. This is in strong contrast to the finding of diffusive equilibration in clinopyroxene phenocrysts with oscillatory zonation, where homogenization takes place in a short time span of months to a few years (Morgan *et al.*, 2004). The oikocrysts from the Norra Ulvö Gabbro were at relatively high temperatures for ~1000 years and should have undergone diffusive equilibration across sectors based on the results of Morgan *et al.* (2004). The sharp compositional boundaries therefore indicate that the sector zonation precludes diffusive exchange and implies a strong structural control on diffusion rates in clinopyroxene.

Oikocryst growth

The first relevant question to be addressed concerning how oikocrysts grow is: where do they grow? In cumulates, oikocrysts are nominally interpreted as having grown after initial accumulation of cumulus grains (chadacrysts). However, chemical and/or textural evidence has led to interpretations that some oikocrysts started to grow prior to accumulation (e.g. Tegner & Wilson, 1995). To include abundant chadacrysts, an oikocryst must grow in a crystal-rich portion of the magma chamber. The simplest explanation is that they grow in the crystal pile at the floor or in an inward growing boundary layer at the roof or walls. An oikocryst that grows in equilibrium with the main magma reservoir will show little or no compositional zoning because its growth will not substantially modify the liquid composition. In the present example, our data clearly indicate that the liquid composition evolves progressively during oikocryst growth—this is especially clear when different domains from the same oikocryst are compared, as discussed below. This is consistent with the conclusions of an earlier study of amphibole oikocrysts (Meurer & Claeson, 2002).

The sector zonation and chemical variation within and between domains make it possible to develop criteria for interpreting how the clinopyroxene oikocrysts of the Norra Ulvö Gabbro grew. Triple points (where three sector zones grow outward from a point) indicate the location of the first oikocryst growth within a domain because growth is always away from these junctions. Similarly, linear sector boundaries indicate the location of early growth within a domain as growth takes place outward from these boundaries. In both cases, the growth of the crystal is away from the junction of two or more sectors. The location of triple points in the sector zonation in the central parts of domains indicates that the oikocrysts nucleated there and not on the surrounding crystals. Initial growth in the interior of domains was also found in an earlier study of an amphibole oikocryst (Meurer & Claeson, 2002). Growth zonation that takes place after sector zonation ceases provides evidence of progressive oikocryst growth. The final crystallization of the oikocryst in a domain takes place at the contacts with the chadacrysts. Some analyses close to cumulus minerals have relatively high concentrations of incompatible trace elements, indicating areas of growth from the evolving liquid in that domain. For example, spot 293cpx3-11 (Electronic Appendix 3), at one edge of a domain, has the highest concentrations of Zr, Ce, and Y and the lowest Ti in that domain. This spot is not distinct in BSE and is interpreted as having grown from the *in situ* evolving interstitial liquid. Sharply bounded blebs at the margins of domains that are distinct in BSE from the rest of the oikocryst do not represent continuous growth of the oikocryst. For example, spot 277cpx1-3 and spots in a nearby domain (277cpx3-26, -35, -36, -37) have extremely high contents of most incompatible elements (Fig. 9, Table 2, Electronic Appendices 2 and 3). These blebs are interpreted as having grown from late-stage liquids that moved through the crystal mush (as discussed below).

The order in which domains were occupied by a growing oikocryst can be determined using a combination of chemical and petrographic criteria. The concurrent crystallization of ulvöspinel during growth of the clinopyroxene oikocrysts depleted the liquid in TiO_2. This, along with a decrease in the Mg-number, is manifest as chemical zonation between domains in the same oikocryst. Domains with lower TiO_2 and Mg-number crystallized later. The enrichment of incompatible elements such as Zr and REE provides a complementary line of chemical evidence to the TiO_2 variations to establish the relative timing of growth of an oikocryst between domains. The overgrowth of sector zones by normal growth zonation and the absence of sector zonation in domains near the margins provide complementary petrographic evidence for understanding the progressive infilling of these domains.

The detailed mapping of sample 293 makes it ideal for assessing how oikocrysts grow. The identification of the different sector zones in each domain was based on their optical characteristics, BSE images, TiO_2 content, Mg-number, and their trace-element contents where available. We identified three different sectors and each is depicted in a different color in Fig. 10. The growth stages of the oikocryst were then determined by comparing these same chemical parameters between like sectors in different domains. As noted above, the TiO_2 content decreases continuously during crystallization as does the Mg-number, whereas incompatible trace elements increase continuously (Figs 7 and 8). The growth pattern is summarized graphically by assigning progressively higher numbers to later grown domains with those domains labeled 1 crystallizing first and those labeled 5 last (Fig. 10). Thus, two domains that are chemically similar and have the highest TiO_2

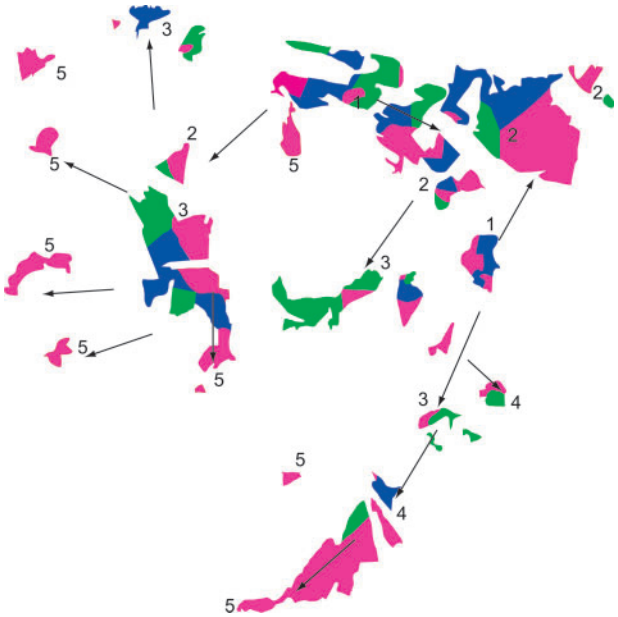

Fig. 10. Color-coded sector zones in an oikocryst from sample 293. The sector zones are defined by optical characteristics and BSE images. They are correlated based on their TiO_2 content, Mg-number (see Figs 5 and 8), and trace-element contents where available. Red indicates low Al, Ti, and high Mg-number; blue indicates high Al, Ti, and low Mg-number; green indicates medium values. The growth directions of the oikocryst between domains are indicated by arrows and were determined by variations in major- and trace-element contents between domains. The growth history is arbitrarily divided into five stages, with 1 being the earliest domains occupied in the section plane and 5 being the last domains filled. The yellow square in photomicrograph Fig. 2d corresponds to the bounding box of this figure and encloses all of the oikocryst studied in this section.

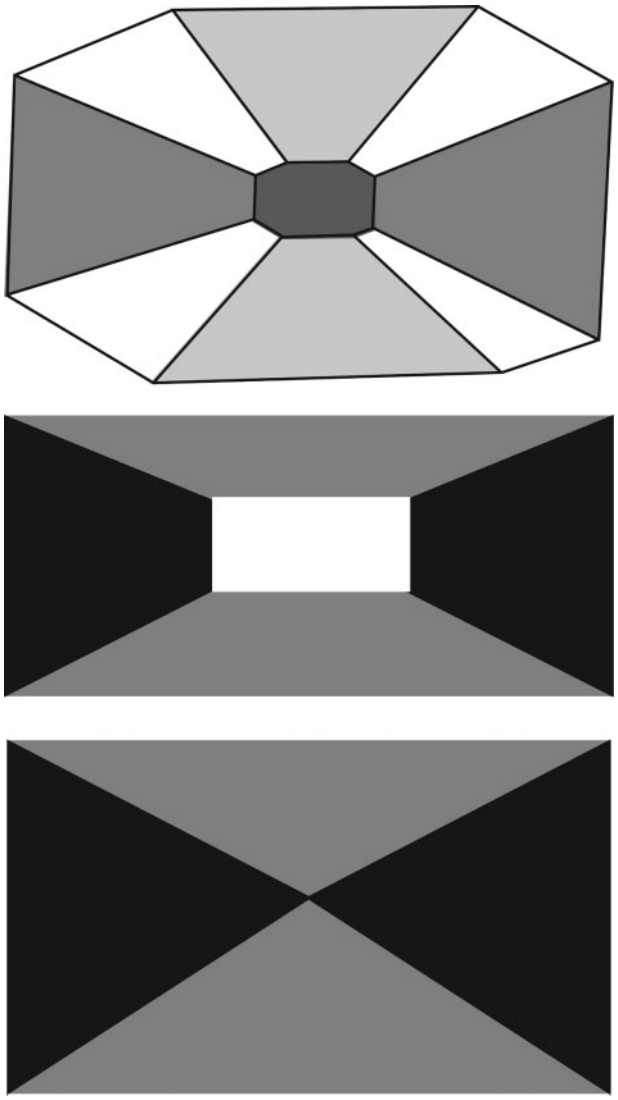

Fig. 11. Idealized clinopyroxene crystals showing development of different sector zones. The top crystal is based on an crystal studied by Brophy *et al.* (1999) and the other two are based on numerous field and experimentally grown crystals. The number and distribution of triple-points and their geometric relations to linear sector-zone boundaries should be noted. These features may be contrasted with the shapes and orientations of similar sector-zone features in Fig. 10.

and Mg-number and lowest incompatible-element concentrations are interpreted as the locations where the oikocryst first started to grow in the section plane (labeled 1 in Fig. 10). The oikocryst grew with a branching morphology, with triple points in domains indicating where the branches pierced that domain. Sections through euhedral sector-zoned clinopyroxene grains have regular orientations of triple points and sector boundaries (e.g. Fig. 11). However, the six triple points in five different domains in the single crystal mapped from sample 293 show no regular orientation and the linear sector-zone boundaries do not conform to any pattern expected from a section through a euhedral sector-zoned crystal (Figs 10 and 11).

Most domains were filled by growth from a branch outside the section plane and so lack piercing points in the section plane. Rapidly growing crystals can have hopper, skeletal or dendritic growth habits (e.g. Donaldson, 1976; Faure *et al.*, 2003). One consequence of dendritic growth is to allow a single crystal to occupy a large volume rapidly via branches. Branching into adjacent domains also precludes nucleation of other clinopyroxene crystals and is likely to cause smaller crystals to be resorbed.

The branches grew into several adjacent domains (labeled 2 in Fig. 10) prior to complete infilling of the initial domains as demonstrated by the growth zonation and blebs at domain margins (Figs 4 and 5). Growth from the branches fills most of the space in newly occupied domains relatively quickly with well-defined crystallographic sectors. This interpretation is based on the observation that the bulk of any given sector in a given domain

is relatively homogeneous and compositionally distinct from the same sector in an adjacent domain. The homogeneity of each domain requires rapid growth as it implies little or no change in the liquid composition. The oikocryst continued to grow, branching into new domains (labeled 3 and 4 in Fig. 10). The final domains filled by the oikocryst (labeled 5 in Fig. 10) are not sector zoned. Most of these domains are at the margins of the crystal as viewed in the section plane, but not all. One number 5 domain is found near the middle of the oikocryst (in the section plane) adjacent to a number 1 domain. This implies either limited connectivity between domains in the section plane or that some domains were not occupied during earlier growth because of their position relative to branch directions. The final growth of the oikocrysts occurred in late-stage channels (forming what we term blebs) between the oikocryst and chadacrysts or host grains.

In several domains, blebs are found that have the highest concentrations of incompatible elements in a given oikocryst. The blebs occur throughout the oikocrysts and are distinct in BSE images as either brighter or darker sharply bounded areas at the edges of domains. The BSE bright blebs have high FeO contents whereas the dark blebs have similar or even higher Mg-numbers compared with the host domain, and both have much lower TiO_2. The dark blebs are invariably adjacent to grains of ulvöspinel. We interpret their composition to have been modified by exchange of Fe and Mg with the oxide grains. This exchange must be a super-solidus process related to the crystallization of the bleb because adjacent parts of the same clinopyroxene crystal in contact with the same oxide grains have not had their compositions discernibly modified. We suggest that these blebs are (1) cross-sections through channels that late-stage liquid moved through and that (2) they remained open throughout the crystallization history of the oikocrysts. The first interpretation is supported by lack of accessory minerals in these blebs. They may contain apatite but lack the albitic plagioclase, K-feldspar, and allanite found in places outside oikocrysts that we interpret to have formed by *in situ* crystallization of interstitial liquid. That these channels remained open throughout the growth of the oikocryst is demonstrated by the blebs having higher incompatible-element concentrations than the more 'normal' parts of the oikocrysts (i.e. higher than any part except for other blebs).

The size and spacing between oikocrysts is governed by the growth rate of the branches relative to the nucleation rate. To grow large oikocrysts, the growth rate must outpace nucleation. Otherwise domains would be populated with several small crystals grown from different nucleation sites. The optimal conditions for crystal growth with minimal nucleation give an upper estimate of the amount of undercooling of <25 K (Dowty, 1980). This is in accordance with suggested amounts of undercooling, of 10–20 or 25 K, to produce sector zoning in clinopyroxene (Kouchi *et al.*, 1983; Mathison, 1987).

The majority of oikocrysts in the Norra Ulvö Gabbro lack contact with other oikocrysts. The few oikocryst–oikocryst contacts we have found show equilibrium interfaces with straight grain boundaries. The vast majority of these contacts are restricted to intersections of domains with a neck-down point between two crystals. However, in the few instances where two oikocrysts meet in the middle of a single domain the interface is straight or slightly undulating. Both of these features suggest that different oikocrysts that start occupying the same domain during growth compete for space. The oikocryst that occupies more of the domain resorbs the competing oikocryst up to the point where the latter occupies a neck-down point or close to such an interface. This is due to surface energy being smaller for the larger crystal, which therefore grows at the expense of the smaller crystals (e.g. Boudreau, 1995; Waters & Boudreau, 1996).

Element partitioning between sector zones

The detailed petrographic and chemical characterization of sector-zoned clinopyroxene crystals provides an excellent opportunity to examine the dependence of trace-element partitioning on minor-element concentrations. Portions of the sector zones that are homogeneous and occupy the bulk of a domain grew from the same liquid, at the same time, so that only differences in minor-element substitutions (Ti, Al, Na) will cause differences in trace-element partitioning. The detailed major- and minor-element mapping provides the basis for selecting homogeneous parts of adjacent sectors for comparison. The quality and quantity of data also allows robust tests of the stoichiometry of the clinopyroxene.

The minor-element composition of the clinopyroxene is most readily examined by calculating the amounts of end-member chemical components. Examination of the major-element composition reveals that the enstatite, ferrosilite, and wollastonite components (En, Fs, Wo) are remarkably invariant within each sample. For example, examination of the 277 analyses of a single clinopyroxene oikocryst in sample 293 reveals the following relative standard deviations for these major components: En = 3·6%, Fs = 4·6%, and Wo = 1·8%. These components account for 93·1% of the composition, with Ca–Ti Tschermaks, jadeite, and acmite components accounting for the remainder. The proportions of the minor components were also calculated from the molecular proportions, normalized to six oxygens, for these 277 analyses as follows:

(1) $Al^{IV} = 2 - Si$ (this assumes full tetrahedral site occupancy);
(2) $Al^{VI} = Al - Al^{IV}$ (all excess Al is taken as Al^{IV});

(3) $CaTiAl_2O_6 = Al^{IV} - 2 \times Ti$ (this component is referred to as Ca–Ti Tschermaks; Ca–Ti Ts);
(4) $NaAlSi_2O_6 = Al^{VI}$ (Al^{VI} is the limiting component for making jadeite);
(5) $NaFe^{3+}Si_2O_6 = Na - Al^{VI}$ (Na excess after making jadeite makes acmite).

The amount of Al^{IV} is essentially equal to $2 \times Ti$ in all analyses with an average excess Al^{IV} of only 0·0046 per formula unit (Electronic Appendix 1). This small difference could correspond to a systematic bias in the SiO_2 content of the analyses of 0·2 wt %—well within the analytical uncertainty. Thus, the Ca–Ti Ts component accounts for essentially all the Ti and Al^{IV}. Na is always present in excess of Al^{VI} and so we arbitrarily ascribe the remaining Na, after making jadeite (Jd), to an acmite (Ac) component. This requires Fe^{3+}, which, when included in a recalculation of the cation proportions, reduces the cation total. The average cation total is 4·0089 with a relative standard deviation of 0·14%. This average total is reduced to ~4·0045 when enough Fe^{3+} is added to make Ac.

The amounts of the minor components in the clinopyroxene are small in an absolute sense (Ca–Ti Ts = 4·24%, Jd = 1·80%, Ac = 0·89% for sample 293) but are large relative to the concentrations of the trace elements and strongly influence their partitioning between different sectors. Five pairs of sectors from different domains provide suitable tests for differences in partitioning behavior (their SEM-EDS identifications in Table 1 are: 180cpx1-35 and 180cpx1-17, 277cpx3-10 and 277cpx3-21, 293cpx2-54 and 293cpx2-59, 293cpx3-21 and 293cpx3-4, 297cpx5-40 and 297cpx5-25). These pairs were analyzed by LA-ICPMS with 100 μm spots from homogeneous regions that are (1) near the boundary between two sector zones, and (2) near the middle of a domain. The Jd component shows little variation between the sectors, and although the Ac component shows some variation it is not systematic. Only the Ca–Ti Ts component shows a systematic variation between sectors and so is interpreted to be the major control on differences in trace-element partitioning. Ratios of trace-element concentrations in the two sectors are analogous to ratios of partition coefficients because the liquid composition is the same for each sector. These ratios can be compared with the ratio of the Ca–Ti Ts component in the high-Ti sector to that in the low-Ti sector, which provides a measure of the compositional contrast between the sectors (Fig. 12a). The results of this comparison are remarkably regular for trace elements with concentrations higher than ~50 ppb. Transition metals (2+) are partitioned equally between the sectors (average ratios are Mn 1·00, Co 1·00, Ni 0·97) whereas all other trace elements are enriched in the high Ti sectors, except for Rb, which is richer in the low-Ti sectors (average Rb ratio 0·37). The REE and Y are all enriched in the high-Ti sectors between ~1·2 and 1·4 times, with perhaps slightly more enrichment in the LREE than in the HREE (Fig. 12). There is a positive correlation between the ratio of the Ca–Ti Ts component and the ratios of the REE (Fig. 12a). Among the 4+ cations Zr shows more enrichment than Ti, and for the 5+ cations Nb shows more enrichment than V.

Experimental studies of clinopyroxene trace-element partitioning (e.g. Hart & Dunn, 1993) have emphasized the importance of coupled substitutions to achieve charge balance for non-divalent cations at the M2 (Ca) and M1 (Mg, Fe) sites. However, there is no general agreement as to the relative importance of the composition of the liquid in governing partitioning (e.g. Nielsen & Drake, 1979; Blundy & Wood, 1991; Dobosi & Jenner, 1999; Hill *et al.*, 2000). Hill *et al.* (2000) conducted experiments at a fixed pressure and temperature, specifically to assess the importance of Al^{IV} [present as $CaAl(Si,Al)O_6$—CaTs] on partitioning of trace elements as a function of their valence. They predicted that with increasing CaTs one should find: (1) an increase in D for HFSE and to a lesser extent the REE; (2) little change in D for alkaline earth; (3) a decrease in D for Co and other 2+ cations substituting into the M1 site, as well as for V^{5+}. Our results are consistent with the first prediction, with Ti, Zr, and Nb all preferentially partitioned into the Ca–Ti Ts-rich sectors and more strongly partitioned into those sectors than the REE. However, our data conflict with the second and third predictions. We find a weak but consistent preference of Sr for the Ca–Ti Ts-rich sectors and a more variable but stronger preference for Ba into those sectors as well. There is little differential partitioning of Mn, Co, and Ni, whereas V concentrations are higher in Ca–Ti Ts-rich sectors. By calculating the ratios of experimental D values of Hill *et al.* (2000) and their corresponding CaTs components, we can directly compare their results with the ratios of the sector zones (Fig. 12b). This comparison reveals a much stronger dependence on CaTs components for Sc, V, and Zr and a more variable dependence of the REE on CaTs than is found for these elements on the Ca–Ti Ts component of the sector zones. The differences between the partitioning behavior seen by Hill *et al.* (2000) in their experiments and that of the sector-zoned crystals of this study could be in part related to differences in the liquid composition. However, differences in the partitioning between different sectors are independent of the liquid composition, as they crystallized from the same liquid. Given the much larger range in liquid compositions and in the ratios of Tschermaks components in the experimental products compared with the sector zones, it is significant that the ratios of the D values are so similar to those of the sector zones. This result suggests that the liquid composition plays a minor role in determining the partitioning behavior.

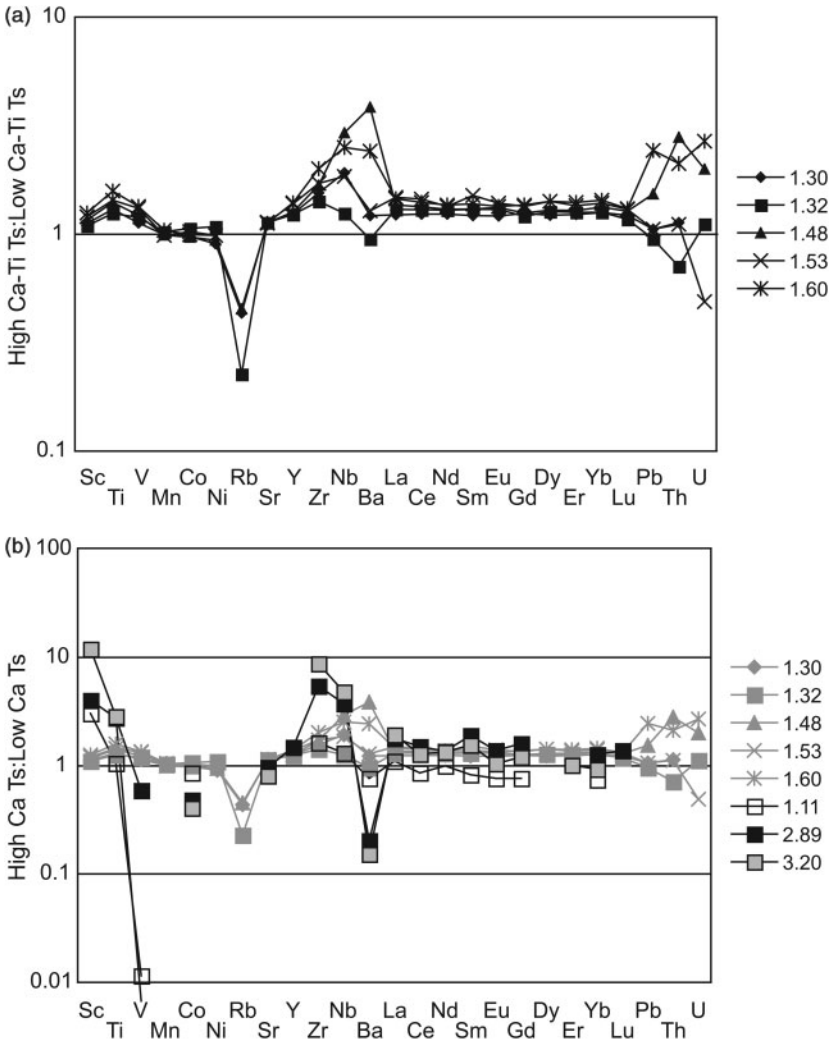

Fig. 12. Normalized trace-element patterns of (a) the ratio of trace-element concentrations in adjacent sectors in a domain coded for the Ca–Ti Ts ratio (high Ti: low Ti) and (b) a comparison of our results (in gray) with those from the experiments of Hill *et al.* (2000) coded based on their CaTs content.

IMPLICATIONS

The presence of the sector zoning in the oikocrysts when combined with detailed chemical mapping provides new insights into how oikocrysts grow. We demonstrate that the growth of oikocrysts does not conform to the idea of simple outward growth from a nucleation point that engulfs and isolates chadacrysts progressively. In the present case, the oikocrysts grew with a branching morphology, and an open framework between the oikocryst and chadacrysts was maintained during nearly the entire growth history of the oikocryst. Although the branches generally grew outward from the nucleation centers, the pattern was not simple and some domains near the centers of the oikocrysts were filled last. This means that oikocrysts need not preserve the texture and compositions of chadacrysts as they grow progressively outward. Additional studies of oikocrysts in gabbroic cumulates are required to evaluate the general nature of these implications and to help build an understanding of their petrological significance.

ACKNOWLEDGEMENTS

Helpful comments were provided by J. Brophy and M. Wilson and are gratefully acknowledged. Discussions with M. E. S. Meurer and Anna Lund improved the content and presentation of this manuscript. The study was supported by Swedish Research Council funding to S.-Å.L. and W.P.M.

SUPPLEMENTARY DATA

Supplementary data for this paper are available at *Journal of Petrology* online.

REFERENCES

Bergantz, G. W. (1995). Changing techniques and paradigms for the evaluation of magmatic processes. *Journal of Geophysical Research* **100**, 17603–17613.

Blundy, J. D. & Wood, B. J. (1991). Crystal-chemical controls on the partitioning of Sr and Ba between plagioclase feldspar, silicate melts and hydrothermal solutions. *Geochimica et Cosmochimica Acta* **55**, 193–209.

Boudreau, A. E. (1995). Crystal aging and the formation of fine-scale igneous layering. *Mineralogy and Petrology* **54**, 55–69.

Brophy, J. G., Whittington, C. S. & Park, Y.-R. (1999). Sector-zoned augite megacrysts in Aleutian high alumina basalts: implications for the conditions of basalt crystallization and the generation of calc-alkaline series magmas. *Contributions to Mineralogy and Petrology* **135**, 277–290.

Claeson, D. T. & Meurer, W. P. (2004). Fractional crystallization of hydrous basaltic 'arc-type' magmas and the formation of amphibole-bearing gabbroic cumulates. *Contributions to Mineralogy and Petrology* **147**, 288–304.

Dobosi, G. & Jenner, G. A. (1999). Petrologic implications of trace element variation in clinopyroxene megacrysts from the Nograd volcanic province, north Hungary: a study by laser ablation microprobe–inductively coupled plasma-mass spectrometry. *Lithos* **46**, 731–749.

Donaldson, C. H. (1976). An experimental investigation of olivine morphology. *Contributions to Mineralogy and Petrology* **57**, 187–213.

Dowty, E. (1980). Crystal growth and nucleation theory and the numerical simulation of igneous crystallization. In: Hargraves, R. B. (ed.) *Physics of Magmatic Processes*. Princeton, NJ: Princeton University Press, pp. 419–485.

Dowty, E., Keil, K. & Prinz, M. (1974). Lunar pyroxene-phyric basalts: crystallization under supercooled conditions. *Journal of Petrology* **15**, 419–453.

Elming, S.-Å. & Mattsson, H. (2001). Post Jotnian basic intrusions in the Fennoscandian Shield, and the break up of Baltica from Laurentia: a palaeomagnetic and AMS study. *Precambrian Research* **108**, 215–236.

Faure, F., Trolliard, G. & Soulestin, B. (2003). TEM investigation of forsterite dendrites. *American Mineralogist* **88**, 1241–1250.

Gorbatschev, R., Solyom, Z. & Johansson, I. (1979). The Central Scandinavian Dolerite Group in Jämtland, central Sweden. *Geologiska Föreningens i Stockholm Förhandlingar* **101**, 177–190.

Hart, S. R. & Dunn, T. (1993). Experimental cpx/melt partitioning of 24 trace elements. *Contributions to Mineralogy and Petrology* **113**, 1–8.

Hawkesworth, C., George, R., Turner, S. & Zellmer, G. (2004). Time scales of magmatic processes. *Earth and Planetary Science Letters* **218**, 1–16.

Hill, E., Wood, B. J. & Blundy, J. D. (2000). The effect of Ca-Tschermaks component on trace element partitioning between clinopyroxene and silicate melt. *Lithos* **53**, 203–215.

Hogmalm, K. J., Söderlund, U., Larson, S.-Å., Meurer, W. P., Hellström, F. A. & Claeson, D. (2006). The Ulvö Gabbro Complex of the 1·27–1·25 Ga Central Scandinavian Dolerite Group (CSDG): intrusive age, magmatic setting and metamorphic history. *Geologiska Föreningens i Stockholm Förhandlingar* **128**, 1–6.

Hollister, L. S. & Gancarz, A. J. (1971). Compositional sector-zoning in clinopyroxene from the Narce area, Italy. *American Mineralogist* **56**, 959–979.

Jensen, B. B. (2000). Partitioning of elements in sector-zoned clinopyroxenes. *Mineralogical Magazine* **64**, 725–728.

Kouchi, A., Sugawara, Y., Kashima, K. & Sunagawa, I. (1983). Laboratory growth of sector zoned clinopyroxenes in the system $CaMgSi_2O_6$–$CaTiAl_2O_6$. *Contributions to Mineralogy and Petrology* **83**, 177–184.

Kushiro, I. (1973). Crystallization of pyroxenes in Apollo 15 mare basalts. *Carnegie Institution of Washington, Annual Report of the Director of the Geophysical Laboratory 1972–1973*, 647–650.

Larsen, L. M. (1981). Sector zoned aegirine from the Ilimaussaq Alkaline Intrusion, south Greenland. *Contributions to Mineralogy and Petrology* **76**, 285–291.

Larson, S.-Å. (1980). Layered intrusions of the Ulvö dolerite complex, Ångermanland, Sweden. PhD thesis, Göteborg University, Institute of Geology..

Larson, S.-Å. & Magnusson, K.-Å. (1976). The magnetic and chemical character of Fe–Ti oxides in the Ulvö dolerite, central Sweden. Geological Survey of Sweden (SGU), Stockholm **C723**, 1–29.

Larson, S.-Å. & Magnusson, K.-Å. (1979). A gravity investigation of the dolerite area on the coast of Ångermanland, Sweden. *Geologiska Föreningens i Stockholm Förhandlingar* **101**, 1–16.

Leung, I. S. (1974). Sector-zoned titanaugites: morphology, crystal chemistry, and growth. *American Mineralogist* **59**, 127–138.

Lundqvist, T. (1990). Beskrivning till berggrundskartan över Västernorrlands län (English summary). Geological Survey of Sweden (SGU), Uppsala **Ba31**, 1–429.

Mathison, C. I. (1987). Pyroxene oikocrysts in troctolitic cumulates—evidence for supercooled crystallisation and postcumulus modification. *Contributions to Mineralogy and Petrology* **97**, 228–236.

Meurer, W. P. & Claeson, D. T. (2002). Evolution of crystallizing interstitial liquid in an arc-related cumulate determined by LA ICP-MS mapping of a large amphibole oikocryst. *Journal of Petrology* **43**, 607–629.

Mogensen, F. (1946). A ferro-ortho-titanate ore from Södra Ulvön. *Geologiska Föreningens i Stockholm Förhandlingar* **68**, 578–588.

Morgan, D. J., Blake, S., Rogers, N. W., DeVivo, B., Rolandi, G., Macdonald, R. & Hawkesworth, C. J. (2004). Time scales of crystal residence and magma chamber volume from modelling of diffusion profiles in phenocrysts: Vesuvius 1944. *Earth and Planetary Science Letters* **222**, 933–946.

Nakamura, Y. (1973). Origin of sector-zoning in igneous clinopyroxenes. *American Mineralogist* **58**, 986–990.

Nielsen, R. L. & Drake, M. J. (1979). Pyroxene – melt equilibria. *Geochimica et Cosmochimica Acta* **43**, 1259–1272.

Skulski, T., Minarek, W. & Watson, E. B. (1994). High-pressure experimental trace-element partitioning between clinopyroxene and basaltic melts. *Chemical Geology* **117**, 127–147.

Tegner, C. & Wilson, J. R. (1995). Textures in a poikilitic olivine gabbro cumulate: evidence for supercooling. *Mineralogy and Petrology* **54**, 161–173.

Van Orman, J. A., Grove, T. L. & Shimizu, N. (1998). Uranium and thorium diffusion in diopside. *Earth and Planetary Science Letters* **160**, 505–519.

Waters, C. & Boudreau, A. E. (1996). A reevaluation of crystal size distributions in chromite cumulates. *American Mineralogist* **81**, 1452–1459.

Watson, E. B. & Liang, Y. (1995). A simple model for sector zoning in slowly grown crystals: implications for growth rate and lattice diffusion, with emphasis on accessory minerals in crustal rocks. *American Mineralogist* **80**, 1179–1187.

Welin, E. & Lundqvist, T. (1975). K–Ar ages of Jotnian dolerites in Västernorrland County, Central Sweden. *Geologiska Föreningens i Stockholm Förhandlingar* **97**, 83–88.